A privileged ER compartment for post-translational heteromeric assembly of an ion channel

Sudharsan Kannan[1], William Kasberg[2], Liliana R. Ernandez[1], Anjon Audhya[2], and Gail A. Robertson[1,*]

1 Department of Neuroscience, School of Medicine and Public Health, University of Wisconsin–Madison, Madison, WI 53705

2 Department of Biomolecular Chemistry, University of Wisconsin-Madison School of Medicine and Public Health, Madison, WI 53706

***Corresponding author:** Gail A. Robertson

Email: garobert@wisc.edu

Author contributions: S.K. and G.A.R. designed research; S.K. and W.K. performed experiments; S.K. and L.R.E. analyzed data; A.A. contributed technology and analytic tools; and S.K. and G.A.R. wrote the paper.

Keywords: arrhythmia, hERG, I_{Kr}, long QT syndrome, condensate, phase separation, protein trafficking, proteostasis, cotranslational assembly, endoplasmic reticulum, oligomerization

Abstract

Mechanisms underlying heterotypic subunit assembly of ion channels and other oligomeric assemblies are poorly understood. In the human heart, heteromeric assembly of two isoforms encoded by the *human ether-à-go-go related gene* (*hERG*) is essential for the normal function of cardiac I_{Kr} in ventricular repolarization, with loss of hERG1b contributing to arrhythmias associated with long QT-syndrome. While hERG1a homomers traffic efficiently to the plasma membrane, hERG1b homomers are retained in the endoplasmic reticulum (ER). When expressed together, the two subunits avidly associate during biogenesis. Seeking rules specifying heteromeric association, we characterized the fate of hERG1b proteins using confocal and superresolution imaging in fixed and live HeLa cells. We found hERG1b sequestered in punctate intracellular structures when expressed alone in HeLa cells. These puncta, driven by an N-terminal “RXR” ER retention signal and phase separation, are distinct from other membranous compartments and proteasomal degradation pathways. The puncta represent a privileged ER sub-compartment distinct from that of ER-retained, type 2 (hERG-based) LQTS mutant proteins, which were rapidly degraded by the proteasome. Introducing hERG1a to cells with preformed hERG1b puncta dissolved these puncta by rescuing extant hERG1b. Rescue occurs by association of fully translated hERG1b with 1a, a surprising finding given previous studies demonstrating cotranslational heteromeric association. We propose that sequestration limits potentially deleterious surface expression of hERG1b homomeric channels while preserving hERG1b for an alternative mode of heteromeric hERG1a/1b channel assembly post-translationally. These findings reveal a surprising versatility of biosynthetic pathways promoting heteromeric assembly.

Introduction

The *human ether-à-go-go-related gene* (*hERG*, or *KCNH2*) encodes the voltage-gated potassium channel Kv11.1, critical for repolarizing the ventricular action potential (1, 2). Loss of hERG function due to unintended channel block or genetic mutations in *KCNH2* can prolong the ventricular action potential, leading to drug-induced or type 2 Long-QT syndrome (LQT2) and sudden cardiac death (1, 2). In addition to cardiac dysfunction, central nervous system diseases such as epilepsy and schizophrenia can also arise from mutations and mis-splicing of hERG (3, 4). The majority of LQT2 mutants and the schizophrenia variant of hERG are trafficking-deficient (5). Thus, understanding the mechanisms that regulate the expression, assembly, and trafficking of hERG channels is of broad biological and medical significance.

In ventricular cardiomyocytes, alternate transcripts encode hERG1a and 1b subunits (or ERG1a and 1b in other organisms), which assemble to form heterotetrameric channels producing the repolarizing I_{Kr} current (6-11). The subunits are identical except in their N-termini, which in ERG1a harbors a Per-Arnt-Sim (PAS) domain (12) that is missing in ERG1b (6). The PAS domain interacts with the C-terminus of the adjacent subunit (13), and perturbation of this interaction alters channel function (14). Expressed independently in heterologous systems, ERG1a subunits form homomeric channels that efficiently traffic to the plasma membrane and produce potassium currents. In contrast, ERG1b homomers traffic inefficiently, producing little or no current (6, 15). When expressed together, ERG1b markedly alters the gating properties of ERG1a currents, providing strong evidence for their coassembly (6). This association appears to occur cotranslationally, based on the following evidence: 1) isolated hERG1a and 1b N-termini interact in vitro in a dose-dependent manner (16); 2) a fragment of the hERG1a N-terminus disrupts oligomerization in cells and impairs core glycosylation, a process known to occur cotranslationally (16, 17); and 3) immunoprecipitation from HEK293 cell or cardiomyocyte

lysates using a hERG1a-specific antibody copurifies nascent hERG1a and 1b subunits along with their encoding mRNAs (18). Together these findings indicate that hERG1a/1b subunit assembly begins cotranslationally, early in biogenesis.

Several lines of evidence underscore the critical role of the heteromeric composition of cardiac I_{Kr}. In canine adult cardiomyocytes, specific antibody staining reveals an approximately equal distribution of the two subunits, localized primarily to the Z line. Similarly, in both canine and human myocardium, western blot analysis using a pan-hERG antibody detects roughly equal amounts of the proteins, supporting the conclusion that cardiac I_{Kr} is predominantly formed by heteromeric hERG1a/1b channels (8). The native current also displays properties more consistent with the heteromer than the hERG1a homomer (19). The hERG1b subunit modulates hERG1a properties, yielding larger currents by accelerating the time course of activation and recovery from inactivation, thus enhancing repolarization (9). Computational studies incorporating these differences in channel gating behavior into a cardiomyocyte model predicted that loss of hERG1b would be pro-arrhythmic (9). This prediction was later validated experimentally: shRNA depletion of hERG1b in cardiomyocytes or introduction of the hERG1a-specific N-terminal PAS domain in trans, which effectively converts native heteromers into hERG1a homomers, leads to prolonged action potential duration (APD) and increased APD variability, two cellular markers of pro-arrhythmia (7).

Previous studies identified an N-terminal, arginine-based endoplasmic reticulum (ER) retention motif (RXR) in hERG1b that is critical for its retention in the ER in the absence of hERG1a (15). In heterologous expression systems, mutating the RXR motif effectively rescues hERG1b from ER retention: hERG1b proteins are fully glycosylated (mature) as assayed by western blot, and they produce robust currents, indicating successful plasma membrane expression (15). Thus, RXR-mediated ER retention ensures that hERG1b subunits predominantly reach the plasma

membrane as components of heteromers, while restricting their expression as homomers. However, the detailed mechanisms of ER retention and rescue of 1b remain unclear.

In this study, we discovered that retained hERG1b proteins are stably sequestered within a privileged ER compartment, which we have termed the “ER sequestration and assembly” (ERSA) compartment. This compartment provides a protected environment, shielding hERG1b from degradation while it awaits assembly with hERG1a, adding a new level of complexity to the previously reported mechanism of cotranslational assembly (16, 18). These findings reveal that biogenesis of heteromeric I_{Kr} channels is prioritized through two distinct mechanisms.

Results

hERG1b is sequestered in intracellular puncta

hERG1a and 1b isoforms exhibit distinct cellular distributions when expressed heterologously. Immunofluorescence confocal microscopy in HeLa cells shows that hERG1a displays a widespread ER signal along with discernible plasma membrane localization, indicative of mature, functional membrane expression (Fig. 1*A*) (20). In contrast, hERG1b forms numerous large intracellular puncta with fluorescence signals measuring 300 nm or greater, detected using automated image analysis (Fig. 1 *B* and *C*; see Methods). Many fewer puncta are observed for hERG1a (Fig. 1*A* and *C*). A corresponding difference is observed when the two isoforms are expressed exogenously at low levels in the more native-like milieu of live cardiomyocytes derived from iPSC cells (Fig. 1 *D*-*F*).

Control experiments confirm that these puncta are not an artifact of the C-terminal tags used for

detection. Untagged hERG1b puncta expressed in HeLa cells show the same distribution when stained with pan-hERG antibody (Fig. S1*A*), and native puncta can also be observed in iPSC-CMs using a pan-hERG antibody (Fig. S1 *B* and *C*), although the lack of availability of a hERG1b-specific antibody precluded isoform assignment. These findings suggest that the puncta serve as the intracellular substrate for the well-documented ER retention of homomeric hERG1b subunits (9, 15, 16).

hERG1b puncta are localized to ER

To determine the subcellular localization of the puncta at superresolution, we imaged hERG1b in iPSC-CMs using two-color stimulated emission depletion (STED) microscopy (Fig. 2). ER labeling was achieved by fusing HaloTag to an ER signal sequence and the KDEL ER retention motif (Halo-KDEL) (21), while hERG1b was tagged with a C-terminal SNAP tag ($1b_{SNAP}$). mRNA was transcribed in vitro from the Halo-KDEL and $1b_{SNAP}$ plasmid constructs and transfected into iPSC-CMs. After 24h, fluorescent labeling of the ER with the JFX650 HaloTag ligand and $1b_{SNAP}$ with the JFX554 SNAP-tag ligand revealed that more than 95% of the puncta were centered within a 50-nm distance from the ER membrane, confirming their ER localization (Fig. 2 *A*-*D*).

Minimal colocalization of hERG1b puncta with other subcellular compartments, including the COPII ER exit compartment, lysosome, or autophagosomes, was observed (Fig. S2). Interestingly, the presence of few autophagosomes (Fig. S2*C*) indicates that hERG1b expression did not trigger significant cellular stress under these conditions (22). These findings establish that hERG1b puncta represent a specialized, ER-resident substructure.

hERG1b is sequestered in a privileged ER compartment

A majority of LQT2-mutant hERG channels fail to mature, accumulating in the ER where they

are ubiquitinated and targeted for proteasomal degradation (5, 23-26). To determine whether ER-sequestered hERG1b meets a similar fate, we compared its retention to that of the trafficking-deficient LQT2 mutant hERG1a-Y611H (24). As expected, when hERG1a-Y611H was transfected into HeLa cells and immunostained, it exhibited intracellular signal with no apparent membrane localization, consistent with its ER retention phenotype; however, it exhibited relatively few puncta compared with hERG1b (Fig. 3 *A*-*C*). To determine relative stabilities, we designed a pulse-chase paradigm to monitor hERG1a-Y611H mutant and 1b degradation. This experiment utilized a plasmid encoding hERG1b-SNAP or hERG1a-Y611H-SNAP; cells were identified with the HaloTag, expressed independently from an internal ribosome entry site (IRES) in the plasmid encoding each isoform. After 24 h transfection, we labeled extant SNAP-tagged proteins with fluorescent ligand JFX650 and then blocked detection of all subsequently synthesized protein using a non-fluorescent ligand (PA-JF-549); thus, proteins labeled and imaged at t=0 could be imaged again 8 h after labeling (Fig. 3*D*). We observed that hERG1b expression was stable with only a modest reduction in fluorescence signal 8 h after labeling (Fig. 3 *E*-*G*). In contrast, hERG1a-Y611H fluorescence was severely reduced, presumably via the action of the proteasome (24) (Fig. 3 *H*-*J*). These findings indicate that hERG1b is harbored in the ER in a privileged compartment we have termed “ER sequestration and assembly compartment,” or ERSA. These experiments show that ERSA is distinct from ER-associated compartments mediating proteolysis and cell quality control in a disease setting.

N-terminal domain of hERG1b drives formation of ER associated condensates

We hypothesized that hERG1b puncta could represent either membrane-enclosed vesicles or condensates arising from multivalent interactions of the cytosolic channel domains (27). To determine whether hERG1b puncta are enclosed by membrane, we used Potomac Yellow dye to ubiquitously label lipids (28, 29). Amid the diffuse staining of organelles, we observed puncta

that we assume represent membranous vesicles. We noted only limited colocalization with fewer than 5% of the Potomac Yellow spots overlapping with hERG1b puncta when center-to-center distance threshold was set to 300 nm or less (Fig. 4 *A* and *B*). We conclude that hERG1b is not concentrated in membranous vesicles.

If ERSA compartments are condensates, we would expect to observe dynamic movement of molecules, which can be assessed using fluorescence recovery after photobleaching (FRAP). With this technique, recovery of fluorescence would reveal the diffusion of fluorescently tagged protein into the bleached area (30). However, we observed no FRAP of puncta for at least 5 min after photobleaching (Fig. S3). Thus, if the puncta are condensates, they are characterized by non-diffusive, gel-like properties such as those observed for TIS granule mesh-like condensates associated with the ER (31, 32). Moreover, the puncta were insensitive to treatment with 1,6-hexanediol, suggesting they may arise from multivalent contacts other than weak hydrophobic interactions (33) (Fig. S4).

Next, given that the differences between hERG1a and 1b occur solely within their N-terminal domains, we assayed for phase separation of GFP-tagged hERG1b N-terminal fragments (1bNT). We found signals in scattered cytosolic puncta and densely concentrated in the nucleus (Fig. 4*C*). The cytosolic puncta were dynamic, exhibiting FRAP although with slow recovery (Fig. 4 *C* and *D*). In silico analysis of hERG1b via Fuzdrop, a proteome-wide ranking of proteins according to their propensity to form condensates (34), reveals likely droplet-forming regions in several positions of hERG1b including the 1b-specific N-terminus (Fig. 4*E*). Future studies will be required to understand the physical properties of the ERSA compartment.

Previous studies showed that hERG1b trafficking is promoted when the $R^{15}XR$ ER retention signal is mutated, as determined by western blot maturation assays and membrane current recordings (15). Given that arginine residues are known to play a critical role in condensate formation (35), we investigated the role of the RXR motif in hERG1b phase separation. Mutating $R^{15}XR$ to $N^{15}XN$ reduced the propensity of 1bNT to form puncta, as quantified by counting the percentage of cells with puncta (Fig. 4 *F and G*). The same mutation in the full-length protein also reduced the number of 1b puncta (Fig. 4 *I-K*). Although more work remains to be done, we propose that the RXR motif in the N-terminal domain facilitates phase separation and the formation of 1b puncta, where the 1b proteins are stored in non-diffusive condensates in the ER.

A similar effect on punctal content is achieved by co-expression with hERG1a, previously shown to rescue hERG1b by "masking" the ER retention signal, with the two subunits serving as co-chaperones (15, 36). In contrast to cells expressing hERG1b alone, those expressing both hERG1a and 1b exhibited fewer puncta and the signal was instead distributed throughout the cytoplasm and plasma membrane (Fig. 4 *I* and *J*). Thus, association with hERG1a dissolves the 1b puncta or prevents their formation.

Sequestered hERG1b is rescued by hERG1a post-translationally

Data to this point do not allow us to discern whether hERG1a rescues hERG1b cotranslationally, i.e., while both subunits are undergoing translation, or post-translationally by associating with fully synthesized, sequestered hERG1b. To make this determination, we created a stable cell line inducibly expressing $hERG1b_{SNAP}$ and observed its behavior in live cells. After inducing $hERG1b_{SNAP}$ for 18 h, we labeled the extant hERG1b proteins with a pulse of fluorescent JFX650 SNAP-tag ligand for 30 min, followed by a nonfluorescent PA-JF-549 SNAP-tag ligand left in the media; this allowed us to track extant hERG1b proteins while ignoring newly

synthesized proteins (Fig. 5*A*). Cells were then transfected with hERG1a-GFP. After 24 h, we observed few hERG1b puncta but clear membrane signal for both hERG1a and 1b compared to mock-transfected cells (Fig. 5 *B-D*). This observation demonstrates that extant hERG1b proteins associate with nascent or newly synthesized hERG1a. Thus, not only are the proteins protected from degradation, but they are also readily available for association with newly synthesized hERG1a.

Discussion

In this study, we demonstrate that hERG1b proteins, in the absence of hERG1a, are selectively retained in punctate ER sequestration and assembly compartments, or *ERSA*. ERSA shields hERG1b proteins from proteasomal degradation, unlike LQT2 mutant hERG1a proteins, which are rapidly degraded. Mutating an N-terminal ER retention signal or co-expressing with hERG1a reduces hERG1b occupancy within ERSA, indicating that this compartment serves as the physical substrate for retained hERG1b. We speculate that ERSA are condensates arising from phase separation of hERG1b at the ER membrane. Notably, hERG1a rescues fully synthesized hERG1b, highlighting a novel role for ERSA in facilitating hERG channel heteromerization beyond previous models of coordinate cotranslation (16, 18). ER sequestration thus acts as a protective mechanism, safeguarding hERG1b from proteasomal degradation and preserving it in space and time until hERG1a becomes available for heteromeric assembly.

Recent studies describe macromolecular protein assembly via several pathways: (1) “co-cotranslational” or simultaneous assembly, where nascent proteins interact as they emerge from the ribosome; (2) “co-post-translational” or sequential assembly, where a fully formed subunit assembles with a different, nascent protein; and (3) “post-translational” assembly where fully formed subunits assemble after translation is complete (37, 38). Previous evidence supports the

idea that hERG1a and 1b assemble through simultaneous cotranslation: in vitro, their heterotypic N-terminal domains associate in a dose-dependent manner; and in cells, disrupting N-terminal interactions disrupts oligomerization and concomitantly diminishes core glycosylation, which serves as a time stamp for early biogenesis (16, 17). Here, we present a new paradigm in which fully synthesized hERG1b can also associate with newly synthesized 1a, as demonstrated for soluble proteins assembling in macromolecular structures in yeast (39, 40). It is unclear whether this association follows a co-post-translational mechanism where 1a is translated near hERG1b, or a strictly post-translational mechanism, in which the hERG1b-containing ERSA compartment is dispersed upon the incursion of full-length hERG1a subunits.

What is the stoichiometry of hERG1b subunits within the ERSA compartment, and how do they assemble with hERG1a? One possibility is that hERG1b subunits assemble into homotetramers, which are escorted out of the ER by tandem interactions with hERG1a homotetramers. This model is reminiscent of the dimeric trafficking of sodium channel pairs (41). Alternatively, hERG1b may reside as homodimers that interact with newly synthesized hERG1a homodimers. This model is inspired by the “dimerization of dimers” mechanism previously established for homomeric assembly of Kv1.3 channels (42). When both hERG1a and 1b mRNAs are locally abundant, the ERSA may play less of a role as cotranslational heterodimers are formed, which then assemble into heterotetramers. Future work determining stoichiometry and composition under different conditions will be required to further illuminate the complexities of assembly.

Liquid-liquid phase separation (LLPS) serves to concentrate proteins and nucleic acids into condensates that regulate many cellular functions and play a critical role in physiology and disease (43, 44). Although studies have focused predominantly on condensates of cytosolic proteins, growing evidence highlights phase separation of membrane proteins, including those

involved in cell signaling (45-47). Our findings suggest that condensates may aid in preserving the integrity of heteromeric hERG channels, creating a protected environment that shields proteins from diffusible components of the proteasomal machinery. This environment, within ERSA, may help manage asymmetric hERG1a and 1b subunit production arising from uneven transcription initiated at their respective promoters (6). By serving as a reservoir, the condensate increases the local concentration of hERG1b, maximizing likelihood of successful association of these rare proteins in the crowded cellular environment.

Decades of research have established the RXR motif as a quality control signal whose masking indicates proper folding and allows ER exit; exposure of the signal triggers protein retention and degradation (15, 48, 49). Our study identifies a potentially new role for this classical motif as a contributor to phase separation, without which ERSA are reduced in number and hERG1b traffics to the plasma membrane. Interestingly, arginine residues are enriched in proteins that undergo phase separation by facilitating protein interactions through salt bridges, cation-pi interactions, or even hydrophobicity (35, 50). It remains to be determined whether RXR-mediated ER retention is achieved by promoting phase separation in other membrane proteins including the NMDA receptor, $GABA_B$ receptor, and K_{ATP} channel subunits (48, 49, 51). Studies of such complexes could help establish a role for phase separation as fundamental to hetero-oligomeric assembly.

In the absence of ER retention, hERG1b homomeric channels traffic to the plasma membrane, where they may disrupt cardiac I_{Kr}. Cardiac I_{Kr} exerts its repolarizing effect late in the ventricular action potential (52). The delay is due to slow activation combined with rapid inactivation, which together suppress the early current; as inactivation recovers, a rebounding tail current repolarizes the cell (1, 2, 53). Homomeric hERG1b channels activate rapidly and exhibit little

inactivation, producing a classic delayed rectifier-type current (6). Such a current would likely counteract the plateau potential and shorten action potential duration (APD). Similar effects are observed with hERG agonists or mutants such as inactivation-impaired S631A, both of which are associated with short QT syndrome, in which the shortened APD allows reentrant arrhythmias in both the ventricle and atria (54-56). Although no pathogenic mutations in the hERG1b RXR signal have been reported, the essential role of hetero-oligomerization underscores its importance in maintaining cardiac rhythm.

Methods

Cell culture

HeLa cells (ATCC, CCL-2) were cultured in 35mm #1.5 glass bottom dishes (Cellvis, D35-14-1.5-N) using DMEM culture media (ThermoFisher, 11995065) supplemented with 10% FBS (ATCC, SCRR-30-2020). HeLa cells were transfected with 500 nanograms of hERG1a or 1b plasmid DNA per 35mm dish with 1 µl of TransIT-X2 Transfection reagent (Mirus Bio, MIR6004), and cells were imaged after 48 h of transfection. Human iCell iPSC-CMs (CDI-FujiFilm) were thawed, plated, and cultured with CDI media according to the manufacturer's specifications. After 10 to 14 days in culture, cells were transfected or fixed for immunostaining followed by imaging. For STED microscopy, mRNAs expressing SNAP tagged hERG1b and HaloTag containing KDEL motif in its C terminus were transfected to iPSC-CM using Lipofectamine MessengerMAX (LMRNA001). 100 nM SNAP-tag ligand JFX650 and 100 nM HaloTag ligand JFX549 were added to the culture media for 30 min, followed by three washes 5 min each using

pre-warmed culture media to remove the free ligand. For membrane labeling, 100 nM Potomac Yellow dye was added to the cell culture media for 15 min, and the cells were imaged live.

Plasmids and Generation of inducible stable cell line

Overexpression plasmids were made from pcDNA3.1 as a backbone. Truncations and insertion of coding sequences of hERG 1a and 1b subunits and fluorescent proteins were performed using In-Fusion® Snap Assembly Master Mix (Takara, 638948). To generate a doxycycline-inducible cell line to express SNAP-tagged hERG 1b, we used a transcription activator-like effector nuclease (TALEN)-mediated targeting system, which incorporated the transgene at the AAVS1 locus (Qian et al., 2014). The puromycin-resistant donor cassette was used to express SNAP-tagged hERG1b, followed by an internal ribosome binding site and a gene encoding mApple. The cassette was transfected into HeLa cells with the two AAVS1-site specific TALEN plasmids at a ratio of 8:1:1, and cells were treated with puromycin (0.75 µg/ml) for approximately 3 weeks. Individual clones were picked and tested for doxycycline-induced expression of SNAP-tagged hERG1b and mApple. For overexpression studies, cells were treated with doxycycline (50 ng/ml) for 24-48 h prior to analysis.

In vitro transcription of mRNAs

pCDNA3.1 plasmid containing SNAP-tagged hERG1b and Halo-KDEL with T7 promotor were linearized using EcoRI restriction enzyme at the 3' end. Linearized plasmids were transcribed using mMESAGE mMACHINE™ T7 Transcription Kit (Invitrogen, AM1344) and poly(A) tailed using E. coli Poly(A) Polymerase (NEB, M0276S).

Immunostaining

Cells were cultured in 12 mm coverslips with #1.5 thickness (Electron Microscopy Sciences 7229004). For labeling using HA (1:1000, Cell Signaling, 3724S), FLAG (1:1000, Sigma, F1804-1MG), Pan-hERG (1:200, Enzo Life Sciences, ALX-251-049-R100), and LC3A/B (1:400, Invitrogen, PA5-22731) antibodies, cells were fixed with 4% paraformaldehyde (PFA) followed by three 5-min washes using PBS. Cells were permeabilized using 0.5% Triton-X-100 followed by 30 min incubation in blocking solution (0.05% Tween-20 and 5% normal goat serum) and overnight incubation at 4^0C with primary antibodies diluted in blocking solution, then incubation with secondary antibodies for 1 h at room temperature. For labeling using Sec24a (1:300, Santa Cruz Biotechnology, sc-169279) and LAMP1(1:100, Invitrogen, eBioH4A3) antibodies, cells were fixed using 100% ice-cold methanol for 10 min at -20^0C, followed by three 5-min washes in PBS and blocking and incubation with primary antibody overnight at 4^0C, then secondary antibody for 1 h at room temperature.

Microscopy and image analysis

Live and Fixed confocal imaging was performed using a Nikon Ti2 spinning disk confocal microscope with a 60x (1.4NA) and 100x (1.45NA) oil immersion objective and Hamamatsu ORCA-Flash4.0 sCMOS camera. Nikon Elements software was used for image acquisition.

Puncta quantification and colocalization analysis were performed using the Imaris (Oxford instruments) spots model. Spot detection was initialized using an estimated diameter of 600 nm and modeled PSF-elongation along the z-axis with an estimated diameter of 1 µm. Initial filtering was applied using the *quality* parameter with an empirically determined threshold to maximize the inclusion of true-positive puncta while excluding background noise. Additionally, spot regions were thresholded based on *local contrast* with an empirically determined threshold to refine spot regions. To ensure consistency and reproducibility, configuration files containing all the

thresholding parameters were generated and applied across images, enabling unbiased segmentation. Further, the spots were filtered for those greater than 300 nm in diameter in the XY plane. Puncta were detected throughout the field of view of the microscopy images and assigned within individual cellular boundaries to quantify puncta on a per-cell basis.

For 1bNT condensate experiments, the number of cells with condensates was quantified manually in a blinded manner. All the quantifications were conducted on raw images, and sample images provided in the figures were deconvoluted using Huygens professional software (Scientific Volume Imaging), using the Classic Maximum Likelihood Estimation (CMLE) algorithm with default settings. Deconvolution was applied evenly to the images used for comparison.

Leica TCS SP8 STED system equipped with highly sensitive HyD detectors and an HC Planapo CS2 100X, 1.4NA oil immersion objective lens was used to acquire STED images. Random regions of interest (25 x 25 µm squares) were selected for image acquisition in each cell. Acquisition parameters were controlled by the Leica Application Suite platform (LASX) and images were deconvolved using Huygens CMLE algorithm. Puncta with ER colocalization analysis was performed using the Imaris spots and surface model. The number of puncta colocalized within the 50 nm, 100 nm, or 200 nm threshold distance from the center of the puncta to the surface was quantified.

ImageJ was used to manually segment the cells, and the integrated density values were exported per cell. Corrected total cell fluorescence (CTCF) was calculated using the formula: CTCF = Integrated Density – (Area of selected cell X Mean fluorescence of background).

Fluorescence recovery after photobleaching (FRAP) studies were performed using a Nikon Ti2 spinning disk confocal equipped with the 488 nm stimulation laser for photobleaching. 100 µs stimulation with maximum power was used to photobleach the region of interest and images were acquired before and after photobleaching in 2-sec intervals for 3-5 min. ImageJ was used to measure the intensity of the photobleaching area and plotted against time.

Pulse-chase analysis of hERG1 subunits

In the pulse-chase analysis, we transfected plasmids containing 1b-SNAP-IRES-Halo or 1a-Y611H-SNAP-IRES-Halo. 24 h after transfection, the proteins were labeled with 100 nM JFX650 SNAP-Tag ligand and 100 nM JF479 HaloTag ligand, followed by three 10-min washes. Subsequently, 100 nM PA-JF549 SNAP-Tag ligand was added and left in the media until the end of the experiment. The live cells were imaged immediately and 8 h after labeling using a Nikon Ti2 spinning disk confocal microscope. The HaloTag expression was used to identify transfected cells even after complete degradation of hERG proteins.

Acknowledgments

We thank members of the Robertson lab, especially Catherine Eichel, Lisandra Flores-Aldama, and Taylor Voelker for critical discussion, Fang Liu for technical support, and members of the Audhya lab for helpful advice and reagents. Zachary T. Campbell and Cynthia M. Czajkowski for reviewing the manuscript and providing suggestions. We thank Luke D. Lavis for providing Janelia Fluor dyes. The work was supported by NIH grants R01-HL131403 and R01-NS081320 (G.A.R.), American Heart Association Predoctoral Fellowship 24PRE1188958 (S.K.) and NIH grants R01 NS124165 and R35 GM134865 (A.A).

References

1. M. C. Sanguinetti, C. Jiang, M. E. Curran, M. T. Keating, A mechanistic link between an inherited and an acquired cardiac arrhythmia: HERG encodes the IKr potassium channel. *Cell* **81**, 299-307 (1995).
2. M. C. Trudeau, J. W. Warmke, B. Ganetzky, G. A. Robertson, HERG, a human inward rectifier in the voltage-gated potassium channel family. *Science* **269**, 92-95 (1995).
3. R. D. Bagnall *et al.*, Exome-based analysis of cardiac arrhythmia, respiratory control, and epilepsy genes in sudden unexpected death in epilepsy. *Ann Neurol* **79**, 522-534 (2016).
4. S. J. Huffaker *et al.*, A primate-specific, brain isoform of KCNH2 affects cortical physiology, cognition, neuronal repolarization and risk of schizophrenia. *Nature Medicine* **15**, 509-518 (2009).
5. C. L. Anderson *et al.*, Large-scale mutational analysis of Kv11.1 reveals molecular insights into type 2 long QT syndrome. *Nat Commun* **5**, 5535 (2014).
6. B. London *et al.*, Two isoforms of the mouse ether-a-go-go-related gene coassemble to form channels with properties similar to the rapidly activating component of the cardiac delayed rectifier K+ current. *Circ Res* **81**, 870-878 (1997).
7. D. K. Jones *et al.*, hERG 1b is critical for human cardiac repolarization. *Proc Natl Acad Sci U S A* **111**, 18073-18077 (2014).
8. E. M. C. Jones, E. C. Roti Roti, J. Wang, S. A. Delfosse, G. A. Robertson, Cardiac IKr Channels Minimally Comprise hERG 1a and 1b Subunits. *Journal of Biological Chemistry* **279**, 44690-44694 (2004).
9. H. Sale *et al.*, Physiological Properties of hERG 1a/1b Heteromeric Currents and a hERG 1b-Specific Mutation Associated With Long-QT Syndrome. *Circulation Research* **103**, e81-e95 (2008).
10. J. P. Lees-Miller *et al.*, Selective Knockout of Mouse ERG1 B Potassium Channel Eliminates I_{Kr} in Adult Ventricular Myocytes and Elicits Episodes of Abrupt Sinus Bradycardia. *Molecular and Cellular Biology* **23**, 1856-1862 (2003).
11. J. P. Lees-Miller, C. Kondo, L. Wang, H. J. Duff, Electrophysiological characterization of an alternatively processed ERG K+ channel in mouse and human hearts. *Circ Res* **81**, 719-726 (1997).
12. J. H. Morais Cabral *et al.*, Crystal structure and functional analysis of the HERG potassium channel N terminus: a eukaryotic PAS domain. *Cell* **95**, 649-655 (1998).
13. W. Wang, R. MacKinnon, Cryo-EM Structure of the Open Human Ether-a-go-go-Related K(+) Channel hERG. *Cell* **169**, 422-430 e410 (2017).
14. C. A. Harley *et al.*, Conformation-sensitive antibody reveals an altered cytosolic PAS/CNBh assembly during hERG channel gating. *Proceedings of the National Academy of Sciences* **118**, e2108796118 (2021).
15. P. Phartiyal, H. Sale, E. M. Jones, G. A. Robertson, Endoplasmic reticulum retention and rescue by heteromeric assembly regulate human ERG 1a/1b surface channel composition. *J Biol Chem* **283**, 3702-3707 (2008).
16. P. Phartiyal, E. M. C. Jones, G. A. Robertson, Heteromeric Assembly of Human Ether-à-go-go-related Gene (hERG) 1a/1b Channels Occurs Cotranslationally via N-terminal Interactions. *Journal of Biological Chemistry* **282**, 9874-9882 (2007).
17. G. Kreibich, B. L. Ulrich, D. D. Sabatini, Proteins of rough microsomal membranes related to ribosome binding. I. Identification of ribophorins I and II, membrane proteins characteristics of rough microsomes. *J Cell Biol* **77**, 464-487 (1978).

18. F. Liu, D. K. Jones, W. J. de Lange, G. A. Robertson, Cotranslational association of mRNA encoding subunits of heteromeric ion channels. *Proc Natl Acad Sci U S A* **113**, 4859-4864 (2016).
19. M. J. McPate *et al.*, hERG1a/1b heteromeric currents exhibit amplified attenuation of inactivation in variant 1 short QT syndrome. *Biochem Biophys Res Commun* **386**, 111-117 (2009).
20. Q. Gong, C. L. Anderson, C. T. January, Z. Zhou, Pharmacological rescue of trafficking defective HERG channels formed by coassembly of wild-type and long QT mutant N470D subunits. *Am J Physiol Heart Circ Physiol* **287**, H652-658 (2004).
21. R. M. Napier, L. C. Fowke, C. Hawes, M. Lewis, H. R. B. Pelham, Immunological evidence that plants use both hdel and kdel for targeting proteins to the endoplasmic reticulum. *Journal of Cell Science* **102**, 261-271 (1992).
22. D. Gozuacik *et al.*, DAP-kinase is a mediator of endoplasmic reticulum stress-induced caspase activation and autophagic cell death. *Cell Death & Differentiation* **15**, 1875-1886 (2008).
23. M. Furutani *et al.*, Novel mechanism associated with an inherited cardiac arrhythmia: defective protein trafficking by the mutant HERG (G601S) potassium channel. *Circulation* **99**, 2290-2294 (1999).
24. Q. Gong, D. R. Keeney, M. Molinari, Z. Zhou, Degradation of trafficking-defective long QT syndrome type II mutant channels by the ubiquitin-proteasome pathway. *J Biol Chem* **280**, 19419-19425 (2005).
25. B. Foo *et al.*, Mutation-specific peripheral and ER quality control of hERG channel cell-surface expression. *Scientific Reports* **9** (2019).
26. P. M. Apaja *et al.*, Ubiquitination-dependent quality control of hERG K⁺ channel with acquired and inherited conformational defect at the plasma membrane. *Molecular Biology of the Cell* **24**, 3787-3804 (2013).
27. Y. G. Zhao, H. Zhang, Phase Separation in Membrane Biology: The Interplay between Membrane-Bound Organelles and Membraneless Condensates. *Dev Cell* **55**, 30-44 (2020).
28. W. R. Legant *et al.*, High-density three-dimensional localization microscopy across large volumes. *Nature Methods* **13**, 359-365 (2016).
29. J. B. Grimm, T. A. Brown, A. N. Tkachuk, L. D. Lavis, General Synthetic Method for Si-Fluoresceins and Si-Rhodamines. *ACS Cent Sci* **3**, 975-985 (2017).
30. N. O. Taylor, M. T. Wei, H. A. Stone, C. P. Brangwynne, Quantifying Dynamics in Phase-Separated Condensates Using Fluorescence Recovery after Photobleaching. *Biophys J* **117**, 1285-1300 (2019).
31. A. A. Hyman, C. A. Weber, F. Julicher, Liquid-liquid phase separation in biology. *Annu Rev Cell Dev Biol* **30**, 39-58 (2014).
32. W. Ma, C. Mayr, A Membraneless Organelle Associated with the Endoplasmic Reticulum Enables 3'UTR-Mediated Protein-Protein Interactions. *Cell* **175**, 1492-1506 e1419 (2018).
33. S. Alberti, A. Gladfelter, T. Mittag, Considerations and Challenges in Studying Liquid-Liquid Phase Separation and Biomolecular Condensates. *Cell* **176**, 419-434 (2019).
34. M. Hardenberg, A. Horvath, V. Ambrus, M. Fuxreiter, M. Vendruscolo, Widespread occurrence of the droplet state of proteins in the human proteome. *Proc Natl Acad Sci U S A* **117**, 33254-33262 (2020).
35. Y. Hong *et al.*, Hydrophobicity of arginine leads to reentrant liquid-liquid phase separation behaviors of arginine-rich proteins. *Nature Communications* **13** (2022).
36. E. B. Rios-Perez *et al.*, A stable cell line inducibly expressing hERG1a/1b heteromeric channels. *J Pharmacol Toxicol Methods* **110**, 107081 (2021).

37. M. Seidel *et al.*, Co-translational assembly orchestrates competing biogenesis pathways. *Nature Communications* **13** (2022).
38. F. Morales-Polanco, J. H. Lee, N. M. Barbosa, J. Frydman, Cotranslational Mechanisms of Protein Biogenesis and Complex Assembly in Eukaryotes. *Annu Rev Biomed Data Sci* **5**, 67-94 (2022).
39. C. D. S. Duncan, J. Mata, Widespread Cotranslational Formation of Protein Complexes. *PLoS Genetics* **7**, e1002398 (2011).
40. C. D. Duncan, J. Mata, Cotranslational protein-RNA associations predict protein-protein interactions. *BMC Genomics* **15**, 298 (2014).
41. J. Clatot *et al.*, Voltage-gated sodium channels assemble and gate as dimers. *Nature Communications* **8** (2017).
42. L. Tu, C. Deutsch, Evidence for Dimerization of Dimers in K+ Channel Assembly. *Biophysical Journal* **76**, 2004-2017 (1999).
43. A. Patel *et al.*, A Liquid-to-Solid Phase Transition of the ALS Protein FUS Accelerated by Disease Mutation. *Cell* **162**, 1066-1077 (2015).
44. S. F. Banani, H. O. Lee, A. A. Hyman, M. K. Rosen, Biomolecular condensates: organizers of cellular biochemistry. *Nature Reviews Molecular Cell Biology* **18**, 285-298 (2017).
45. S. Banjade, M. K. Rosen, Phase transitions of multivalent proteins can promote clustering of membrane receptors. *Elife* **3** (2014).
46. X. Su *et al.*, Phase separation of signaling molecules promotes T cell receptor signal transduction. *Science* **352**, 595-599 (2016).
47. M. Zeng *et al.*, Phase Transition in Postsynaptic Densities Underlies Formation of Synaptic Complexes and Synaptic Plasticity. *Cell* **166**, 1163-1175 e1112 (2016).
48. N. Zerangue, B. Schwappach, Y. N. Jan, L. Y. Jan, A new ER trafficking signal regulates the subunit stoichiometry of plasma membrane K(ATP) channels. *Neuron* **22**, 537-548 (1999).
49. M. Margeta-Mitrovic, Y. N. Jan, L. Y. Jan, A Trafficking Checkpoint Controls GABAB Receptor Heterodimerization. *Neuron* **27**, 97-106 (2000).
50. R. M. Vernon *et al.*, Pi-Pi contacts are an overlooked protein feature relevant to phase separation. *eLife* **7** (2018).
51. D. B. Scott, T. A. Blanpied, G. T. Swanson, C. Zhang, M. D. Ehlers, An NMDA Receptor ER Retention Signal Regulated by Phosphorylation and Alternative Splicing. *The Journal of Neuroscience* **21**, 3063-3072 (2001).
52. M. C. Sanguinetti, N. K. Jurkiewicz, Two components of cardiac delayed rectifier K+ current. Differential sensitivity to block by class III antiarrhythmic agents. *J Gen Physiol* **96**, 195-215 (1990).
53. T. Shibasaki, Conductance and kinetics of delayed rectifier potassium channels in nodal cells of the rabbit heart. *J Physiol* **387**, 227-250 (1987).
54. A. Zou, Q. P. Xu, M. C. Sanguinetti, A mutation in the pore region of HERG K⁺ channels expressed in Xenopus oocytes reduces rectification by shifting the voltage dependence of inactivation. *The Journal of Physiology* **509**, 129-137 (1998).
55. I. M. Herzberg, M. C. Trudeau, G. A. Robertson, Transfer of rapid inactivation and sensitivity to the class III antiarrhythmic drug E-4031 from HERG to M-eag channels. *The Journal of Physiology* **511**, 3-14 (1998).
56. M. C. Sanguinetti, HERG1 channel agonists and cardiac arrhythmia. *Current Opinion in Pharmacology* **15**, 22-27 (2014).

Figure Legends

Fig. 1. hERG 1b is sequestered in intracellular puncta. (A) Confocal images of fixed and immunostained HeLa cells transfected with *hERG1a* or (B) *hERG1b* plasmids; (C) quantification of the number of puncta per cell; data are mean ± s.d., n= 36 cells per condition, analyzed with Student's t-test (**** indicating p<0.0001); (D) Confocal live cell images of iPSC-CM transfected with 1a-GFP or (E) 1b-GFP; (F) quantification of number of puncta per cell; data are mean ± s.d., n=18 cells for $1a_{GFP}$, 12 cells for $1b_{GFP}$, analyzed with Student's t-test (**** indicating p<0.0001); Scale bar: 10 μm in large image and 2 μm in the inset.

Fig. 2. hERG1b puncta are localized to ER. (A-C) STED microscopy of iPSC-CM transfected with mRNAs encoding $hERG1b_{SNAP}$ labeled with JFX554 (magenta) and ER marker Halo-KDEL labeled with JFX650 (cyan); (D) quantification of colocalization events thresholded with three different distances between the center of hERG1b puncta and the surface of the ER; data are mean ± s.d., n= 16 regions of interest (see Methods); (E) cartoon of ER localization of hERG1b puncta. The scale bar is 10 μm for (A) and 500 nm for (B,C).

Fig. 3. hERG1b is sequestered in a privileged compartment. (*A*) Immunostaining of HeLa cells transfected with $hERG1b_{HA}$ or (*B*) $hERG1a\text{-}Y611H_{HA}$; (*C*) quantification of the number of puncta per cell; data are mean ± s.d., n=33 for hERG1b, n=26 for 1a-Y611H, analyzed with a Student t-test (**** indicating p<0.0001) ; (D) experimental design for the pulse-chase experiment; (*E*) $hERG1b_{SNAP}$-transfected live cells imaged 0 h after labeling and (*F*) 8 h after labeling; (*H*) $hERG1a\text{-}Y611H_{SNAP}$-transfected live cells imaged 0 h after labeling and (*I*) 8 h after labeling; (*G,J*) quantification of corrected total fluorescence intensity (CTFT) per cell; data are mean ± s.d., n= 35-40 cells per condition, analyzed with a Student's t-test (**** indicating p<0.0001); inset on the lower left of (*E,F,H,I*) shows the Halo-tag expression used to identify the transfected cells. Scale bar: 10 μm for large images (A-I) & 2 μm for insets (A, B).

Fig. 4. hERG1b ER trafficking rescue is accompanied by dissolution of hERG1b condensates. (*A*) Confocal images of live HeLa cells expressing hERG 1b (magenta) stained with Potomac-Yellow dye (cyan) labeling membranes; scale bar: 10 μm in the large image and 2 μm in the insets (i, ii); (B) quantification of percentage of number of hERG1b puncta colocalizing within 250 nm with Potomac-labeled membranous puncta (n=15 cells); (C) GFP tagged hERG1b amino-terminal domain (1-64 residues) undergoes phase separation, with fluorescence recovery after photobleaching of individual puncta; (D) quantification of normalized fluorescence intensity after photobleaching; data are mean ± SEM; n= 13 puncta from different cells in representative experiment of three total; (E) droplet-promoting regions in 1b identified by Fuzdrop, which includes the N-terminal domain. (F) Confocal images of HeLa cells expressing $1bNT^{N15XN}{}_{GFP}$; scale bar: 10 μm in large image and 1 μm in inset; (G) graph showing % cells with puncta in 1bNT-WT and 1bNT-N_{15}XN mutant protein-expressing cells. 1bNT-WT exemplar is shown in *C*; n= 3 independent wells per condition, with an average from 50 cells in each well, data are mean ± s.d., analyzed with a Student's t-test (*** indicating p<0.001); (H) confocal images of HeLa cells expressing FLAG-tagged hERG1b alone, (I) hERG1b with N^{15}XN mutation, and (*J*) co-expression of WT hERG1a and hERG1b; (*K*) quantification of the number of puncta per cell; data are mean ± s.d. (n= 30 cells per condition) analyzed with a one-way ANOVA (**** indicating p<0.0001); scale bar: 10 μm in large image and 2 μm in inset.

Fig. 5. Sequestered 1b proteins can be rescued by newly expressed 1a. (*A*) Experimental design; (*B*) mock-transfected cells showing hERG1b puncta; (*C*) 1a-transfected cells showing hERG1b signal in or near plasma membrane in live cell imaging; (*D*) quantification of the number of puncta per cell. Data are mean ± s.d., n= 35-42 cells per condition, and analyzed with a Student's t-test (**** indicating p<0.0001). Scale bar: 10 μm in large image and 2 μm in inset.

Fig. 1.

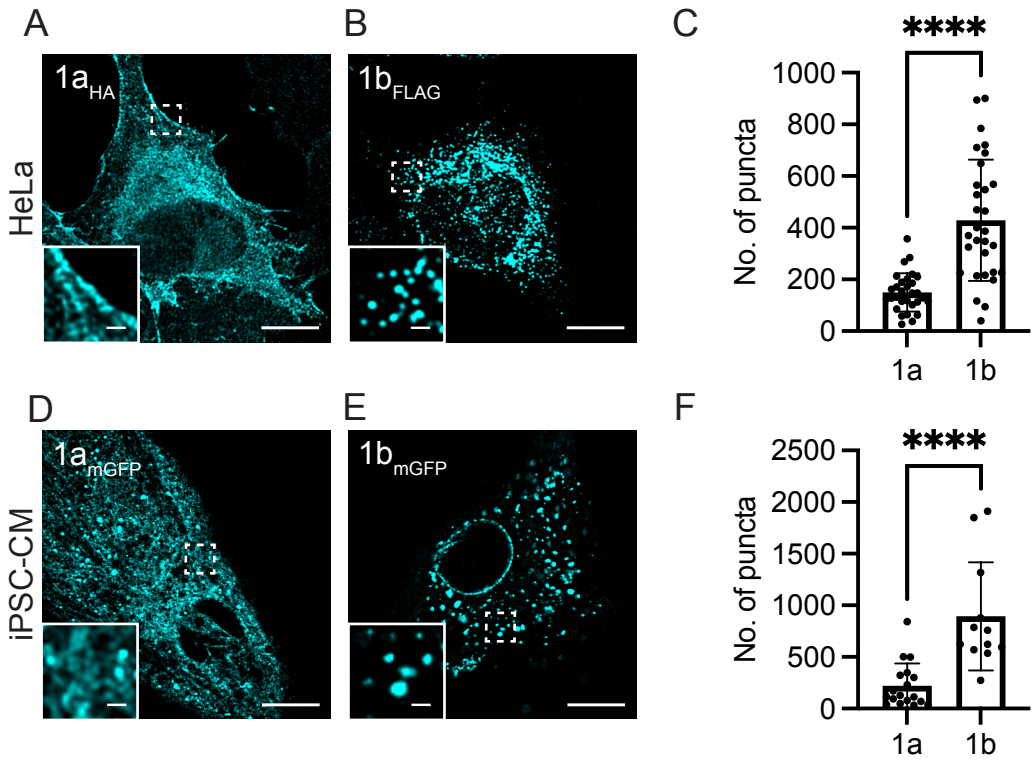

Fig. 2.

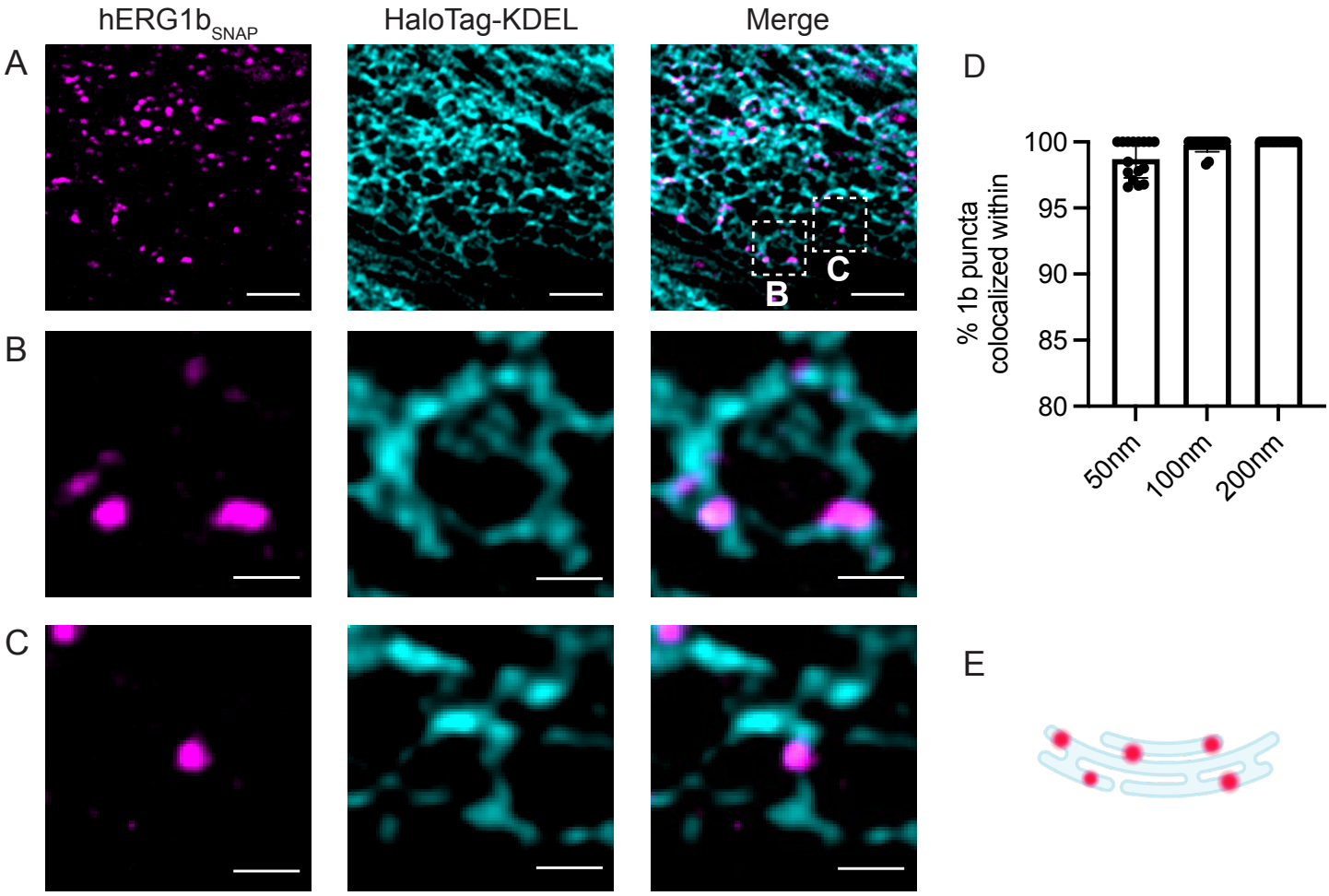

Fig. 3.

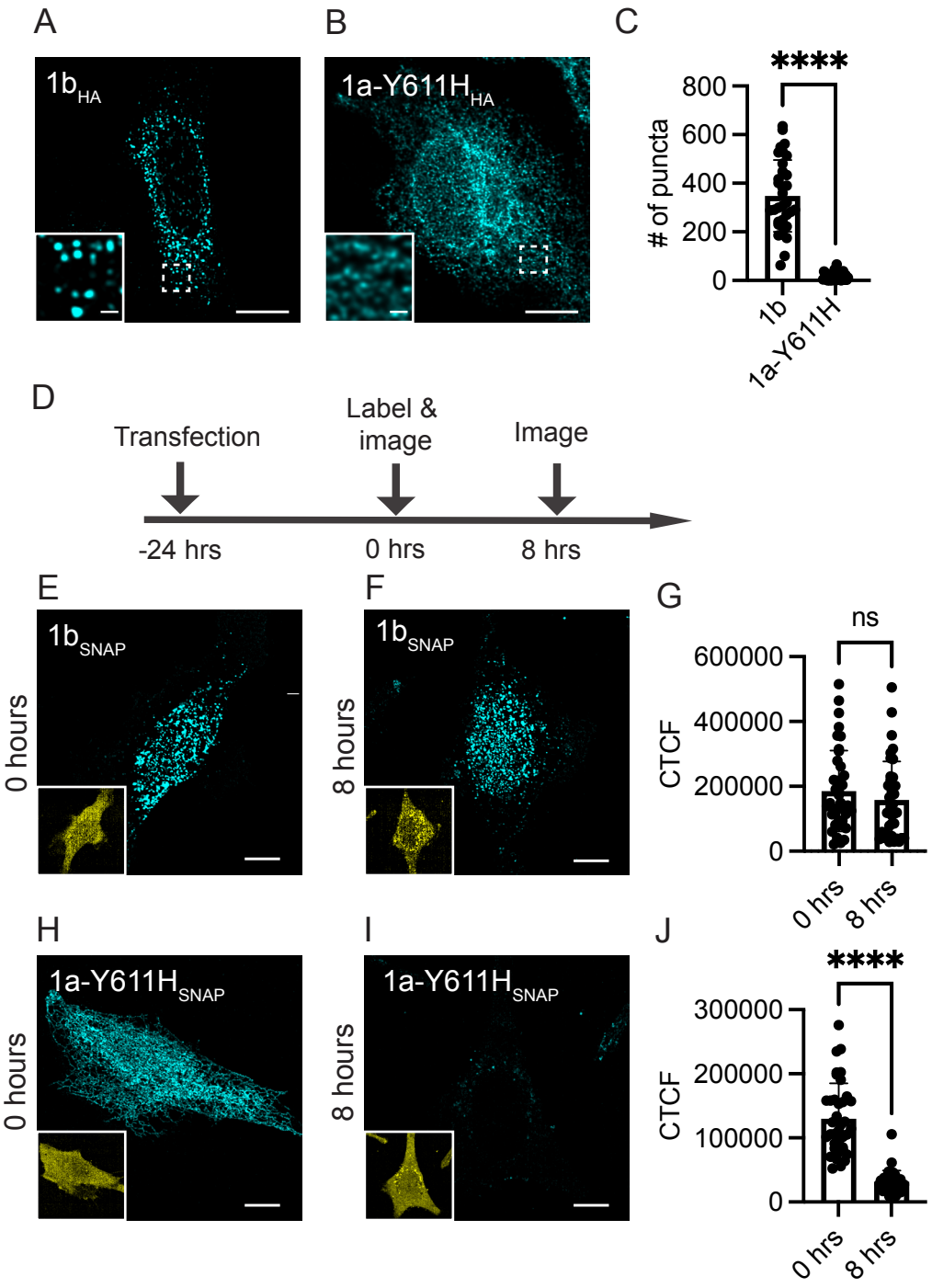

Fig. 4.

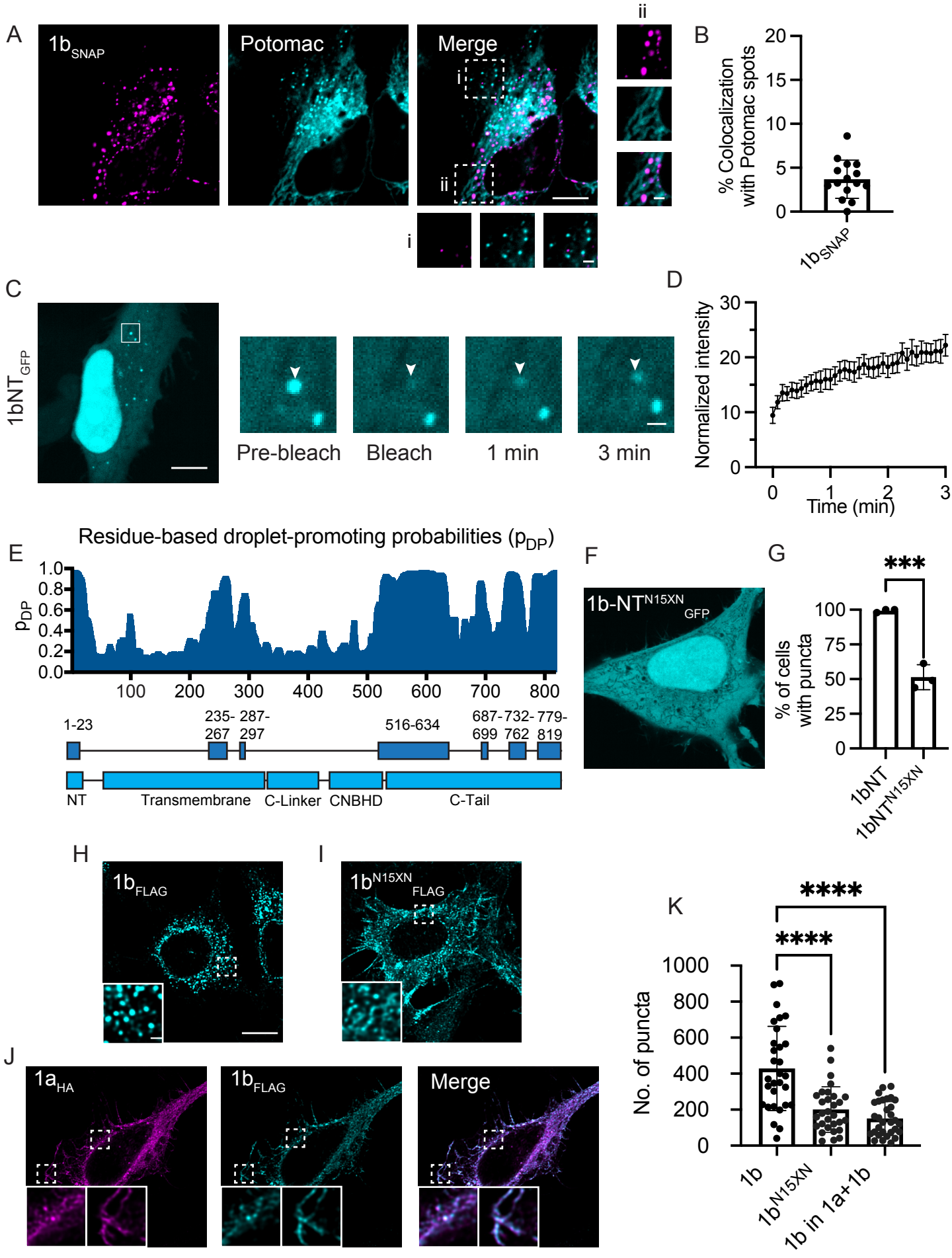

Fig. 5.